PNAS RESEARCH ARTICLE | CELL BIOLOGY OPEN ACCESS

Unconventional secretion of PARK7 requires lysosomal delivery via chaperone-mediated autophagy and specialized SNARE complex

Biplab Kumar Dash[a], Yasuomi Urano[a,1], Yuichiro Mita[b], Yuki Ashida[b], Ryoma Hirose[a], and Noriko Noguchi[a,1]

Affiliations are included on p. 11.

Edited by Hugo Bellen, Baylor College of Medicine, Houston, TX; received July 23, 2024; accepted March 9, 2025

PARK7/DJ-1, a redox-sensitive protein implicated in neurodegeneration, cancer, and inflammation, exhibits increased secretion under stress. We previously demonstrated that, as a leaderless protein, PARK7 relies on an unconventional autophagy pathway for stress-induced secretion. The current study delves deeper into the mechanisms governing PARK7 secretion under oxidative stress triggered by the neurotoxin 6-hydroxydopamine (6-OHDA). Here, we revealed that 6-OHDA-induced autophagic flux is critical for PARK7 secretion. Downregulation of syntaxin 17 (STX17), a SNARE protein crucial for autophagosome-lysosome fusion and cargo degradation, hindered PARK7 secretion. Likewise, impairing lysosomal function with bafilomycin A1 (BafA1) or chloroquine (CQ) diminished PARK7 release, highlighting the importance of functional lysosomes, potentially in the form of secretory autolysosomes, in PARK7 release. We also found that 6-OHDA appeared to promote the unfolding of PARK7, allowing its selective recognition by the chaperone HSPA8 via KFERQ-like motifs, leading to PARK7 translocation to the lysosomal membrane through LAMP2 via chaperone-mediated autophagy (CMA). Additionally, a dedicated SNARE complex comprising Qabc-SNAREs (STX3/4, VTI1B, and STX8) and R-SNARE SEC22B mediates the fusion of PARK7-containing autolysosomes with the plasma membrane, facilitating the extracellular release of PARK7. Hence, this study uncovers a mechanism where 6-OHDA-induced autophagic flux drives the unconventional secretion of PARK7, involving CMA for PARK7 translocation to lysosomes and specialized SNARE complexes for membrane fusion events.

PARK7/DJ-1 | unconventional secretion | SNAREs | secretory autolysosome | chaperone-mediated autophagy

Significance

The findings from this study significantly advance our understanding of the unconventional autophagy-mediated secretion of the multifunctional protein PARK7/DJ-1, which is implicated in various pathological conditions, including neurodegenerative diseases, cancer, and inflammation. The elucidation of the selective translocation of PARK7 to the lysosomal lumen via chaperone-mediated autophagy, as well as the identification of the dedicated Soluble N-ethylmaleimide-sensitive factor attachment protein receptor (SNARE) complex responsible for the fusion of PARK7-containing vesicles with the plasma membrane, provide crucial insights into the autophagy-dependent secretion of PARK7 under oxidative stress. These mechanistic insights hold the potential to inform the development of targeted therapeutic strategies aimed at modulating PARK7 secretion in the context of PARK7-related pathologies.

Eukaryotic cells secrete proteins through a conventional pathway involving the endoplasmic reticulum (ER) and Golgi apparatus. However, some proteins without an N-terminal signal peptide utilize unconventional secretion to bypass or partially use this system. These pathways include direct translocation across the plasma membrane, ABC transporter-mediated secretion, intracellular vesicle-mediated exocytosis, and Golgi-bypass secretion (1, 2). Unconventionally secreted proteins regulate diverse extracellular processes, including immunity, neurodegeneration, and cancer (2, 3). While the conventional pathway is well defined, unconventional secretion mechanisms remain an active area of research.

Autophagy, a cellular recycling process, maintains homeostasis by degrading cytoplasmic components via lysosomes (4). Under stress, cytoplasmic cargoes such as damaged organelles and protein aggregates are sequestered into autophagosomes for degradation (5). Autophagosome biogenesis is initiated by adenosine monophosphate-activated protein kinase (AMPK), mechanistic target of rapamycin (mTOR), and Unc-51-like autophagy-activating kinase 1 (ULK1) signaling, while the VPS34 complex generates phosphatidylinositol 3-phosphate (PI3P) on autophagic membranes, recruiting WIPI2 and the autophagy-related (ATG) protein ATG5-ATG12-ATG16L1 complex for LC3 lipidation (6–10). LC3 undergoes conversion to its active form, LC3-II, after ATG4B cleaves LC3 to expose a C-terminal glycine, which is then lipidated by ATG7 and ATG3 in conjunction with the ATG5-ATG12-ATG16L1 complex. This conversion is a hallmark of nascent autophagic membranes (11). ATG16L1 also binds to FIP200, a component of the ULK1 complex, ensuring coordination between these core autophagy subsystems (12). As autophagosomes mature, they acquire a specific Qa-Soluble N-ethylmaleimide-sensitive factor attachment protein receptor (SNARE) protein, syntaxin 17 (STX17), which interacts with the coiled-coil domain of ATG14, forming a stable complex with another Qbc-SNARE, SNAP29. This SNARE complex and PI3P tethering by ATG14 facilitate fusion with the lysosomal R-SNARE VAMP8 (13, 14). This interaction drives the fusion of autophagosomes with lysosomes through a four-helix bundle

The authors declare no competing interest.

This article is a PNAS Direct Submission.

[1]To whom correspondence may be addressed. Email: yurano@mail.doshisha.ac.jp or nnoguchi@mail.doshisha.ac.jp.

This article contains supporting information online at https://www.pnas.org/lookup/suppl/doi:10.1073/pnas.2414790122/-/DCSupplemental.

Published May 6, 2025.

SNARE complex formation, generating autolysosomes where the captured material is degraded.

Autophagy involves two primary mechanisms: nonselective (or bulk) degradation, which indiscriminately engulfs and degrades cytoplasmic components to sustain cell viability during nutrient scarcity until resources are restored, and selective degradation, which identifies explicitly and eliminates potentially harmful or superfluous cargo. Selective autophagy distinguishes itself from nonselective autophagy by targeting specific substrates, often marked by ubiquitin or other molecular signals. These substrates are recognized by specialized autophagy receptors, such as sequestosome-like receptors, including the well-studied SQSTM1/P62 (sequestosome 1). Additionally, certain forms of selective autophagy, such as ER-phagy and PTEN-induced putative kinase 1 (PINK1)-independent mitophagy, rely on membrane-bound receptors activated by specific cellular signals (15). In contrast, chaperone-mediated autophagy (CMA) precisely delivers cytosolic proteins with KFERQ-like motifs to lysosomes for degradation (16). The cytosolic chaperone HSPA8/HSC70 and cochaperones recognize these proteins and shuttle them to the lysosomal receptor LAMP2A for breakdown (16, 17).

While autophagy is traditionally known for its role in cellular housekeeping by degrading cytoplasmic components within lysosomes, recent research suggests a more diverse functionality. Several key autophagy machinery components appear to have been repurposed for a distinct function: unconventional protein secretion via secretory autophagy (18–20). While the precise mechanism for this switch remains elusive, fundamental differences exist between the two pathways. Secretory autophagy utilizes core ATG proteins for autophagosome formation and amphisome generation (fusion of autophagosomes with late endosomes/MVBs). In contrast to degradative autophagy, IL-1β secretion via secretory autophagy involves the specialized receptor TRIM16 and the ER-Golgi intermediate compartment (ERGIC) R-SNARE SEC22B for IL-1β sequestration into autophagosomes. These SEC22B-containing autophagosomes bypass STX17-mediated lysosomal fusion and facilitate IL-1β secretion with plasma membrane SNAREs STX3/4 and SNAP23/29 (21). Notably, several intracellular proteins, including yeast acyl-CoA-binding protein (22), IL-1β and IL-18 (18, 21, 23), small heat shock protein α-Crystallin B (24), nuclear protein HMGB1 (25), and Alzheimer's disease-associated ubiquitin mutant (26) have been reported to be released via secretory autophagy. Nonetheless, the current knowledge regarding the involvement of SNARE proteins in secretory autophagy is elusive.

Parkinson's disease (PD) protein PARK7/DJ-1 is a ubiquitously expressed multifunctional protein fundamentally known for protecting mitochondria through its antioxidant activity, promoting cell survival, and regulating gene expression (27–30). Compromised PARK7 function is linked to neurodegeneration, cancer, stroke, and inflammation (31–36). Despite lacking a dedicated N-terminal signal sequence, PARK7 can be released from the cell, playing crucial roles in physiological and pathological processes, including antioxidative effects (37), neuroprotection (38), angiogenesis, osteogenesis (39), and even the degradation of aggregated transthyretin (40). Elevated expression and increased PARK7 secretion into the extracellular fluid, including cerebrospinal fluid, breast milk, and blood, are observed in patients with various pathophysiological conditions such as atopic dermatitis, cancer, strokes, melanoma, allergies, multiple sclerosis, and early PD (40–47). The involvement of PARK7 in disease progression highlights it as a potential biomarker for diagnosis, monitoring, and prognosis. However, the exact mechanism by which PARK7 exits the cell remains largely unknown.

Our previous work demonstrated that exposure of mouse embryonic fibroblasts (MEF) and human neuroblastoma SH-SY5Y cells to the neurotoxin 6-hydroxydopamine (6-OHDA) triggered oxidative stress, leading to increased autophagy and subsequent PARK7 secretion (48). That study suggested the involvement of the unconventional secretory autophagy pathway in PARK7 release, as evidenced by the requirement for core autophagic membrane biogenesis proteins like ATG5, ATG9, and ATG16L1. However, several critical aspects of this pathway, including the molecular events and the regulatory steps underlying PARK7 secretion, remain to be elucidated. The present study delves deeper into the unconventional secretory autophagy pathway responsible for PARK7 release upon 6-OHDA treatment. Our findings provide evidence that autophagic flux is essential for this process. We find a specific requirement for the lysosomal fusion SNARE protein STX17, but not its partner SNAP29, in PARK7 secretion. It appears that the KFERQ-like motifs of PARK7 are used for selective translocation of monomeric PARK7 to the lysosomal lumen, like those recognized by the CMA pathway, leading to its secretion. Furthermore, we unveil a dedicated SNARE complex comprising plasma membrane Q-SNAREs (STX3/4, VTI1B, and STX8) and R-SNARE SEC22B, orchestrating the final step of PARK7 release.

Results

6-OHDA Induces Unconventional PARK7 Secretion in HeLa Cells. This study extends our investigation into human cervical carcinoma HeLa cells to explore PARK7 secretion outside the central nervous system. We collected conditioned serum-free medium following 6-OHDA treatment and precipitated the secreted proteins using trichloroacetic acid precipitation (Fig. 1*A*). Western blot (WB) analysis was then performed to evaluate the levels of PARK7 present in the conditioned medium. Consistent with our prior observations, 6-OHDA treatment induced a dose-dependent increase in PARK7 secretion in HeLa cells (Fig. 1*B*), suggesting a consistent pattern across distinct cell lines. To ensure that PARK7 release resulted from secretion and not cell death, we measured lactate dehydrogenase (LDH) activities, a cytoplasmic marker, in the media. Minimal LDH release was observed (Fig. 1*C*), indicating no significant cell death or membrane disruption under the experimental conditions.

Next, we investigated whether PARK7 secretion occurs via the conventional ER-Golgi pathway. We employed brefeldin-A (BFA) to block ER-to-Golgi trafficking. As expected, BFA blocked the secretion of the conventionally secreted protein fibronectin 1 (FN1) (Fig. 1*D*). However, 6-OHDA-induced PARK7 secretion was not affected by BFA treatment. This observation suggests that 6-OHDA-induced PARK7 secretion utilizes a pathway independent of the conventional secretory route.

To investigate the possibility of exosome-mediated PARK7 secretion (cargo delivery via multivesicular bodies, MVBs), we isolated extracellular vesicles, including exosomes, from the conditioned media using ultracentrifugation. WB analysis confirmed a high enrichment of exosomes in isolated pellets, as evidenced by the exosome-specific marker TSG101 (*SI Appendix*, Fig. S1*A*). Notably, PARK7 was exclusively detected in the soluble fraction (SF) and absent from the TSG101-positive pellets. Additionally, treatment with GW4869, an exosome release inhibitor, while suppressing the secretion of an exosomal protein CD63, did not suppress 6-OHDA-induced PARK7 secretion (*SI Appendix*, Fig. S1*B*). These results collectively suggest that 6-OHDA-induced PARK7 secretion utilizes an unconventional pathway independent of the conventional secretory route and exosome release.

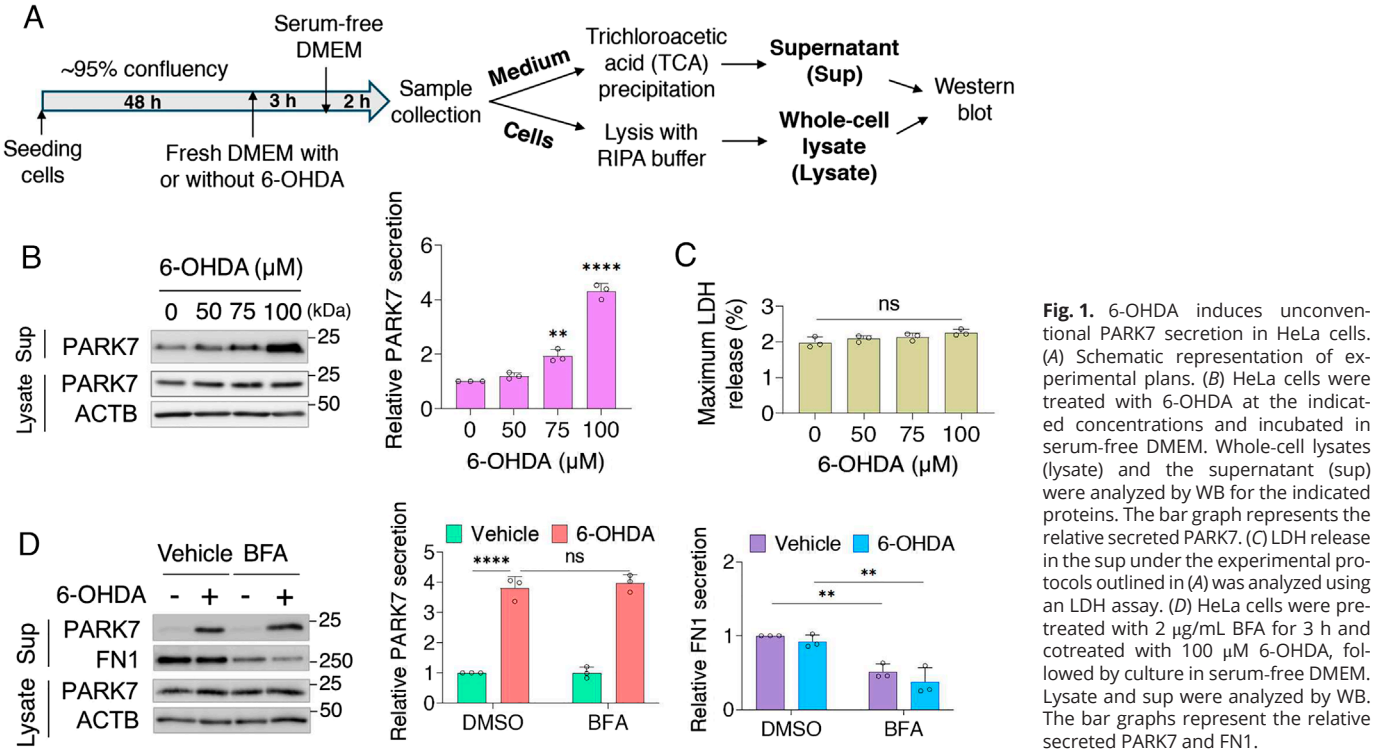

Fig. 1. 6-OHDA induces unconventional PARK7 secretion in HeLa cells. (*A*) Schematic representation of experimental plans. (*B*) HeLa cells were treated with 6-OHDA at the indicated concentrations and incubated in serum-free DMEM. Whole-cell lysates (lysate) and the supernatant (sup) were analyzed by WB for the indicated proteins. The bar graph represents the relative secreted PARK7. (*C*) LDH release in the sup under the experimental protocols outlined in (*A*) was analyzed using an LDH assay. (*D*) HeLa cells were pretreated with 2 μg/mL BFA for 3 h and cotreated with 100 μM 6-OHDA, followed by culture in serum-free DMEM. Lysate and sup were analyzed by WB. The bar graphs represent the relative secreted PARK7 and FN1.

6-OHDA Treatment Induces Autophagy and Promotes Autophagosome–Lysosome Fusion. Next, we investigated the effect of 6-OHDA on autophagy in HeLa cells to understand its potential role in PARK7 secretion. To avoid potential confounding effects of serum-free media on autophagy flux monitoring, we analyzed lysates from cells treated with 6-OHDA for 3 h. We stimulated HeLa cells with increasing doses of 6-OHDA and probed for autophagosomal marker LC3B and autophagic substrate SQSTM1. Our results revealed a dose-dependent increase in LC3B-II and a decrease in SQSTM1 upon 6-OHDA treatment (Fig. 2*A*), indicating activation of autophagy.

Our observation of autophagosome accumulation (as indicated by increased LC3B-II) upon 6-OHDA treatment could be due to upregulated autophagic flux or a blockage in downstream autophagic steps, such as impaired autophagosome-lysosome fusion or diminished lysosomal degradation capacity. To differentiate between these scenarios, we monitored autophagic flux using bafilomycin A1 (BafA1) and chloroquine (CQ), inhibitors of lysosomal acidification and autophagosome-lysosome fusion (49, 50). Combined treatment with 6-OHDA and either inhibitor significantly increased LC3B-II levels compared to the respective inhibitor alone (Fig. 2*B*). These data suggest that 6-OHDA is an inducer of autophagic flux.

To further understand 6-OHDA-induced autophagic flux, we employed HeLa cells transiently expressing mRFP-GFP tandem fluorescent-tagged LC3 (tfLC3), a reporter dissecting the autophagosome maturation process (51). This reporter leverages the distinct pH sensitivities of its red fluorescent protein (mRFP) and green fluorescent protein (GFP) tags to distinguish between autophagosomes and autolysosomes. Under neutral pH conditions, mRFP and GFP fluorescence are visible in newly formed autophagosomes, appearing as yellow puncta in merged images. Conversely, upon autophagosome-lysosome fusion, the acidic lysosomal environment quenches GFP fluorescence (due to its higher pKa) while preserving RFP fluorescence as red puncta, thus indicating autolysosomes (51). As shown in the merged panels of Fig. 2*C*, 6-OHDA treatment significantly increased the number of yellow (arrowheads) and red (arrows) puncta compared to the control group. These findings, consistent with observations in SH-SY5Y and MEF cells (48), demonstrate that 6-OHDA activates autophagy in HeLa cells, leading to increased autophagosome formation, enhanced autophagosome-lysosome fusion, and ultimately increased autophagic flux.

PARK7 Secretion Requires Autophagy Initiation. To investigate the requirement of autophagy for PARK7 secretion, we utilized MRT68921, an inhibitor targeting the early stage of autophagy by blocking ULK1. Treatment with MRT68921 significantly diminished 6-OHDA-induced LC3B-II formation (Fig. 3*A*) and PARK7 secretion (Fig. 3*B*). Further supporting this notion, we evaluated PARK7 secretion in HeLa cells lacking FIP200 (52). As expected, as a component of the ULK1-ATG13-FIP200 autophagosome formation complex, FIP200-deficient HeLa cells ($FIP200^{-/-}$ exhibited minimal changes in LC3B-II conversion upon 6-OHDA treatment (*SI Appendix*, Fig. S2*A*). Additionally, PARK7 secretion was suppressed in $FIP200^{-/-}$ even in response to 6-OHDA treatment (Fig. 3*C*). These findings, along with our previous report demonstrating the requirement of autophagy membrane biogenesis proteins like ATG5, ATG9, and ATG16L1 in PARK7 secretion (48), strongly support the notion that autophagy induction is essential for PARK7 secretion.

Conversely, to explore the impact of increased autophagy on PARK7 secretion, we treated HeLa cells with rapamycin, an autophagy inducer. As expected, rapamycin treatment increased LC3B-II levels (*SI Appendix*, Fig. S2*B*) and concurrently enhanced PARK7 secretion (Fig. 3*D*) dose-dependently, indicating that promoting autophagy can further enhance PARK7 secretion.

We then employed N-acetylcysteine (NAC), an antioxidant that inhibits oxidative stress by combating reactive oxygen species generated by 6-OHDA treatment. NAC effectively suppressed 6-OHDA-induced autophagy (decreased LC3B-II) (Fig. 3*E*) and nearly abolished PARK7 secretion (Fig. 3*F*) compared to control

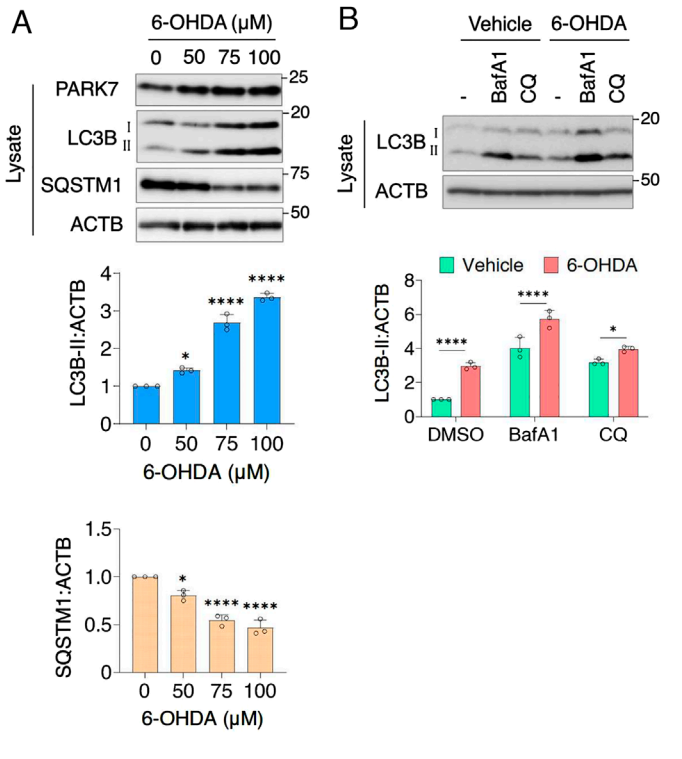

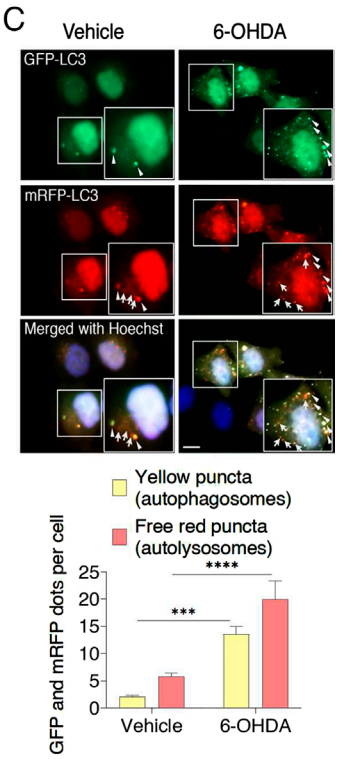

Fig. 2. 6-OHDA treatment induces autophagy and promotes autophagosome-lysosome fusion. (*A*) HeLa cells were treated with 6-OHDA at the indicated concentrations and lysates were analyzed by WB. The bar graph illustrates the relative LC3B-II and SQSTM1 intensities normalized by ACTB. (*B*) HeLa cells were pretreated with 100 nM BafA1 or 5 μM CQ for 2 h and cotreated with 100 μM 6-OHDA. Lysates were analyzed by WB. The bar graph illustrates the relative LC3B-II intensities normalized by ACTB. (*C*) HeLa cells transiently transfected with tf-LC3 plasmids were treated with 100 μM 6-OHDA and observed under a fluorescence microscope for GFP (green), mRFP puncta (red), and nuclei (Hoechst, blue). Boxed areas represent enlarged views. Arrowheads point to autophagosomes (GFP and RFP puncta). Arrows point to autolysosomes (mRFP puncta only). The bar chart represents the quantification of yellow (number of autophagosomes) and free red (number of autolysosomes) puncta in the merged panels. (Scale bar, 10 μm.)

conditions. These findings collectively suggest that autophagy induction is essential for PARK7 secretion, with stress-induced autophagy enhancing its release, highlighting the interplay among cellular stress, autophagy, and PARK7 secretion.

Autophagosome-Lysosome Fusion Is Essential for 6-OHDA-Induced PARK7 Secretion. Since 6-OHDA treatment induces autophagy flux, we explored the involvement of lysosomes in PARK7 secretion. To evaluate the impact of lysosomal activity on basal PARK7 secretion, we treated HeLa cells with CQ or a combination of CQ and NH_4Cl, inhibiting autophagosome-lysosome fusion and hindering autolysosomal degradation. These treatments effectively blocked autolysosomal degradation, as evidenced by the accumulation of both LC3B-II and SQSTM1 (Fig. 4*A*), confirming impaired autophagic flux. Notably, lysosomal inhibition led to a marked increase in intracellular PARK7 accompanied by decreased secretion, suggesting active lysosomal regulation of PARK7 homeostasis. Furthermore, the inhibition of autophagosome-lysosome fusion by BafA1 or CQ treatment almost abolished 6-OHDA-induced PARK7 secretion (Fig. 4*B*). In support of these findings, subcellular fractionation experiments revealed a substantial accumulation of PARK7 in LAMP1-positive lysosomal fractions following 6-OHDA treatment (Fig. 4*C*). Complementary immunofluorescence analysis showed enhanced colocalization of PARK7 with the late endosomal/lysosomal marker LAMP2 under 6-OHDA treatment (*SI Appendix*, Fig. S3*A*). These findings highlight lysosomal involvement as a key regulatory mechanism governing PARK7 secretion during 6-OHDA-induced oxidative stress.

We next investigated the role of STX17 in PARK7 secretion. STX17 deficiency blocks autophagic flux, evidenced by LC3B-II accumulation even under normal growth conditions (14). We employed *STX17* knockout HeLa cells ($STX17^{-/-}$) and siRNA-mediated Stx17 knockdown in MEF cells. In both approaches, we observed LC3B-II and SQSTM1 accumulation (*SI Appendix*, Fig. S3 *B* and *C*), indicating impaired autolysosome formation. Additionally, PARK7 secretion was substantially suppressed in these STX17-deficient cells compared to controls, even under 6-OHDA stimulation (Fig. 4 *D* and *E*). These findings suggest that STX17-mediated autophagosome-lysosome fusion is essential for efficient PARK7 secretion.

Autophagosome-Lysosome Fusion in 6-OHDA-Induced PARK7 Secretion Is Independent of STX17-SNAP29 or STX17-SNAP47 SNARE Complex. After demonstrating that STX17 is essential for 6-OHDA-induced PARK7 secretion, we sought to elucidate the roles of specific SNARE proteins within the complex machinery responsible for autophagosome-lysosome fusion. We initially focused on SNAP29, a Qbc-SNARE protein known to interact with STX17 and mediate autophagosome-lysosome fusion (14). We employed siRNA knockdown of Snap29 in MEF cells and evaluated its effect on Park7 secretion under 6-OHDA treatment. Snap29 knockdown exhibited LC3B-II and Sqstm1 accumulation (Fig. 5*A*), indicating inhibited autophagic flux like STX17 knockdown. However, unlike Stx17, Snap29 knockdown did not decrease Park7 secretion (Fig. 5*B*). Intriguingly, it even resulted in a slight increase in 6-OHDA-induced Park7 secretion. We further investigated Snap47 using a similar knockdown approach in MEF cells. Consistent with Snap29 knockdown, Snap47 knockdown triggered LC3B-II accumulation (Fig. 5*C*), whereas 6-OHDA treatment elevated Park7 secretion (Fig. 5*D*). These intriguing findings suggest that, although PARK7 secretion relies on the autophagosomal Qa-SNARE STX17 for autolysosome formation, the Qbc-SNAREs SNAP29 and SNAP47 appear not essential in the context of 6-OHDA-induced PARK7 secretion.

6-OHDA Does Not Affect Lysosomal Integrity. We next investigated the role of lysosomes in PARK7 secretion beyond their involvement in autophagic flux. First, we examined whether 6-OHDA treatment affects lysosomal integrity or triggers lysosomal membrane permeabilization (LMP)-induced autophagy. Using the pH-sensitive LysoTracker Red probe, we observed a decrease in red fluorescence puncta intensity upon BafA1 treatment (Fig. 6*A*). However, the overall red fluorescence signal remained unchanged

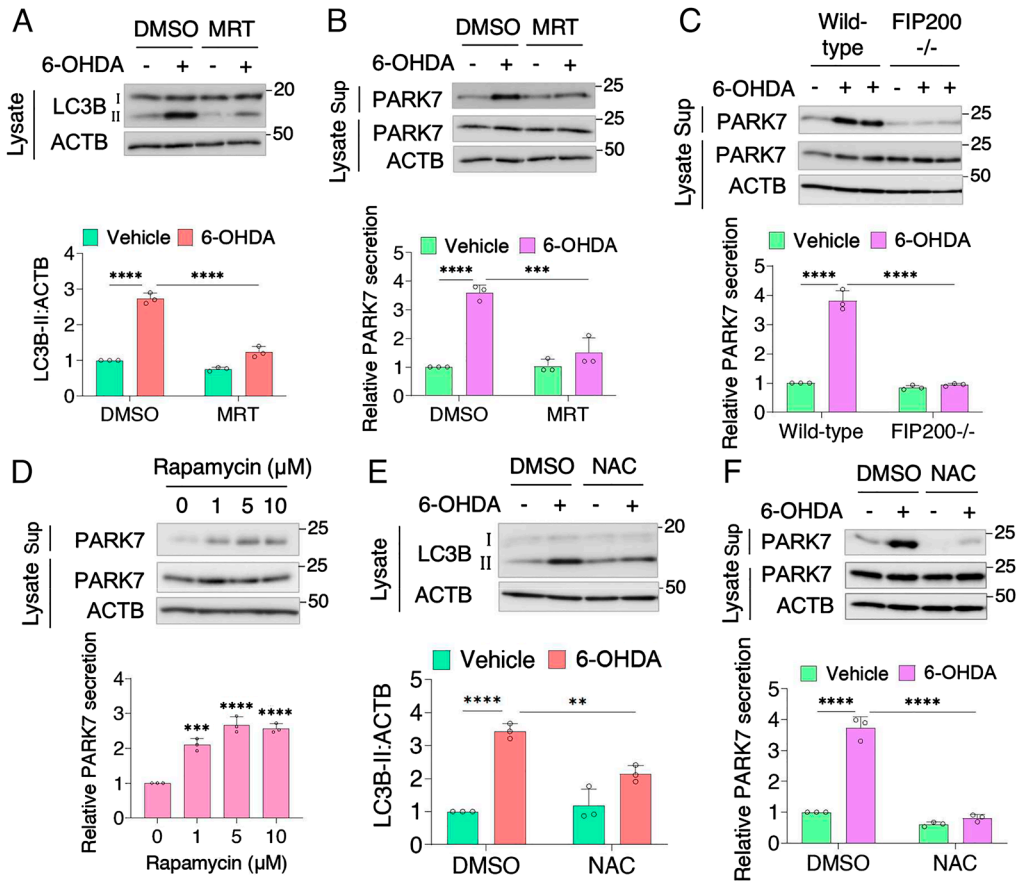

Fig. 3. PARK7 secretion requires autophagy initiation. (*A* and *B*) HeLa cells were pretreated with 2 μM MRT68921 for 30 min and cotreated with 100 μM 6-OHDA (*A*), followed by culture in serum-free DMEM (*B*). Lysates and sup were analyzed by WB. The bar graphs illustrate the relative LC3B-II intensities normalized by ACTB and the relative secreted PARK7. MRT, MRT68921. (*C*) Wild-type or FIP200$^{-/-}$ HeLa cells were treated with 100 μM 6-OHDA and cultured in serum-free DMEM. Lysates and sup were analyzed by WB. The bar graph represents the relative secreted PARK7. (*D*) HeLa cells were pretreated with rapamycin at the indicated concentrations for 3 h and incubated in serum-free DMEM. Lysates and sup were analyzed by WB. The bar graph represents the relative secreted PARK7. E&F) HeLa cells were treated with 2 mM NAC for 2 h and cotreated with 100 μM 6-OHDA (*E*), followed by culture in serum-free DMEM (*F*). Lysates and sup were analyzed by WB. The bar graphs illustrate the relative LC3B-II intensities normalized by ACTB and the relative secreted PARK7.

upon 6-OHDA treatment compared to the control condition. These data indicate that 6-OHDA does not cause a significant lysosomal pH shift or major disruption of lysosomal integrity. Immunofluorescence analysis with the LMP marker galectin-3 (LGALS3) further supported this result. Treatment with L-leucyl-L-leucine methyl ester (LLOMe), a known inducer of LMP, resulted in punctate LGALS3 staining that colocalized with the lysosomal marker LAMP1 (Fig. 6*B*). Conversely, 6-OHDA treatment did not induce LGALS3 puncta formation, indicating an absence of apparent LMP. These findings indicate that 6-OHDA exposure, within the parameters of our experiment, does not induce LMP or compromise lysosomal homeostasis.

We explored the involvement of other cellular protein degradation pathways in 6-OHDA-induced PARK7 secretion. Treatment with MG132, a proteasome inhibitor accumulating ubiquitinated proteins, did not significantly affect either intracellular or secreted PARK7 levels (*SI Appendix*, Fig. S4). This observation suggests that the ubiquitin–proteasome system, another primary protein degradation pathway, does not contribute to PARK7 secretion in this context. Moreover, MG132 treatment did not modify the effect of 6-OHDA on PARK7 levels, further confirming that PARK7 is not a substrate for ubiquitin-proteasomal degradation, even under 6-OHDA stimulation. These findings suggest that PARK7 degradation and secretion are linked explicitly to lysosomal function.

A Unique Set of SNARE Members Mediates PARK7 Release in the Extracellular Environment. To understand the mechanism underlying the involvement of autolysosomes in the unconventional secretion of PARK7, we investigated the role of specific SNARE proteins in 6-OHDA-induced PARK7 secretion. According to the SNARE hypothesis depicted in Fig. 7*A*, a SNARE complex comprises four membrane proteins (Qa-, Qb-, Qc-, and R-SNAREs) mediating membrane fusion. We investigated Sec22b, an R-SNARE protein linked to Golgi-ER trafficking. Recent studies suggest its involvement in autophagosome formation and unconventional protein secretion via autophagosome-plasma membrane fusion (21, 53). Interestingly, Sec22b knockdown using siRNA in MEF cells did not affect autophagosome formation, as measured by LC3B-II protein levels (*SI Appendix*, Fig. S5*A*). However, Sec22b knockdown considerably diminished Park7 secretion (Fig. 7*B*), underscoring Sec22b's essential role in regulating Park7 secretion.

Based on the interaction of Sec22b with plasma membrane syntaxins (54), we sought to identify the specific Qabc-SNARE partners essential for PARK7 release. We screened previously reported plasma membrane SNAREs involved in fusion events (21). Single knockdown of the plasma membrane Qa-SNAREs syntaxin 3 (Stx3) or syntaxin 4 (Stx4) partially suppressed Park7 secretion in MEF cells, whereas combined knockdown of both Stx3 and Stx4 abolished 6-OHDA-induced secretion (Fig. 7*C* and *SI Appendix*, Fig. S5*B*), indicating their critical roles. We then investigated Qbc-SNARE candidates. Knockdown of Snap23 did not affect 6-OHDA-induced PARK7 secretion, while Snap29 knockdown slightly increased it, similar to Fig. 5*B* (Fig. 7*D* and *SI Appendix*, Fig. S5*C*). Combined knockdown of Snap23 and Snap29 also did not affect PARK7 secretion, suggesting that neither Snap23 nor Snap29 is essential for this process.

Since functional lysosomes are crucial for PARK7 secretion, we examined the involvement of endolysosomal SNAREs: Vti1a/b (Qb-SNAREs) and syntaxin 8 (Stx8, Qc-SNARE). Knockdown of Vti1b, but not Vti1a, and Stx8 significantly suppressed 6-OHDA-stimulated Park7 secretion in MEF cells (Fig. 7 *E* and *F* and *SI Appendix*, Fig. S5 *D* and *E*). To determine whether these SNAREs form a functional complex, we performed coimmunoprecipitation

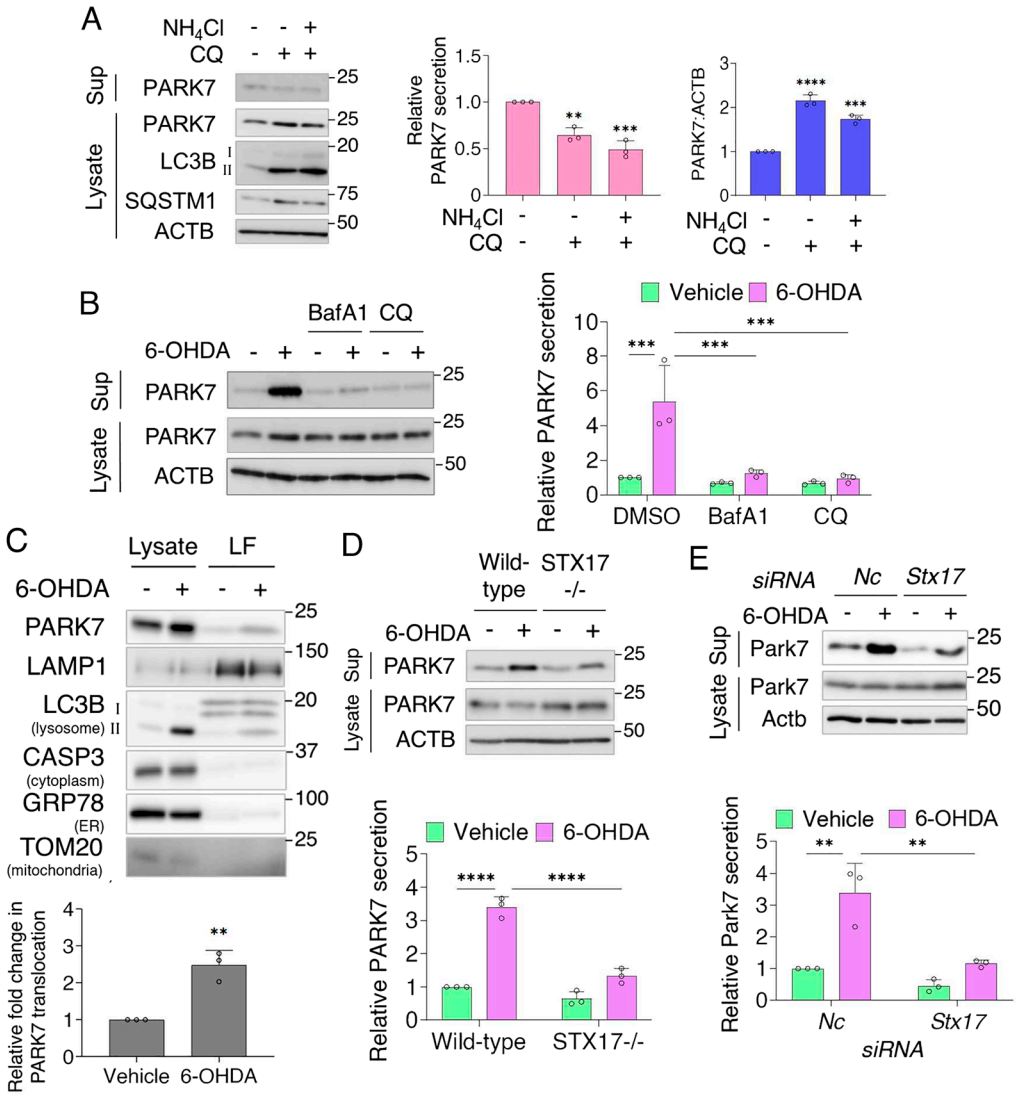

Fig. 4. Autolysosome formation is essential in 6-OHDA-induced PARK7 secretion. (*A*) HeLa cells were treated with 5 μM CQ only or in combination with 10 mM NH_4Cl for 24 h and cultured in serum-free DMEM. Lysates were analyzed by WB. The bar graphs illustrate the relative secreted PARK7, and the relative intracellular PARK7 normalized by ACTB. (*B*) HeLa cells were pretreated with 100 nM BafA1 or 5 μM CQ for 2 h and cotreated with 100 μM 6-OHDA, followed by culture in serum-free DMEM. Lysates and sup were analyzed by WB. The bar graph represents the relative secreted PARK7. (*C*) HeLa cells were treated with 100 μM 6-OHDA for 3 h, followed by lysosome isolation. An equal fraction of lysosomal fractions was compared with 3 μg of lysates for each experimental condition by WB. The bar chart represents the relative fold change in PARK7 translocation to lysosomes. LF, lysosomal fraction. (*D*) Wild-type or $STX17^{-/-}$ HeLa cells were treated with 100 μM 6-OHDA and cultured in serum-free DMEM. Lysates and sup were analyzed by WB. The bar graph represents the relative secreted PARK7. (*E*) MEF cells transfected with siRNAs targeting *Stx17* or *Nc* were treated with 100 μM 6-OHDA and cultured in serum-free DMEM. Lysates and sup were analyzed by WB. The bar graph represents the relative secreted Park7. *Nc*, negative control.

(co-IP) using an anti-Stx8 antibody. The results confirmed that Stx3, Stx4, Sec22b, and Vti1b coprecipitated with Stx8, with increased precipitation upon 6-OHDA treatment (Fig. 7*G*). To rule out nonspecific interactions and validate the specificity of our IP assay, we used Snap47 and Hspa8 as negative controls, neither of which coprecipitated with the target SNAREs. These findings suggest the existence of a Sec22b-containing QabcR–SNARE complex (Stx3/4, Vti1b, Stx8, and Sec22b) that potentially mediates Park7 secretion into the extracellular environment.

To further validate the SNARE complex formation observed in co-IP experiments, we employed AlphaFold2 multimer analysis. This advanced tool predicts high-quality 3D structures of protein complexes, including their binding interfaces, by identifying regions of sequence similarity (55). The AlphaFold2 analysis (*SI Appendix*, Fig. S5 *F* and *G*) mirrored the co-IP data, revealing structural support for the proposed Sec22b-Stx3/4-Vti1b-Stx8 complex. These data identified a Sec22b-mediated SNARE complex involving endolysosomal and plasma membrane SNAREs as potential vesicular transport machinery for Park7 secretion triggered by 6-OHDA.

KFERQ-Like Motifs Contribute to PARK7 Secretion Via CMA. To understand the specific route of 6-OHDA-induced PARK7 translocation into autophagic vesicles, we explored the potential role of Transmembrane P24 Trafficking Protein 10 (TMED10). A recent study identified TMED10 as a transmembrane channel protein facilitating the translocation of multiple leaderless cargoes, including mature IL-1 family members, from the ERGIC lumen to secretory vesicles (56). Given the involvement of the ERGIC-derived R-SNARE SEC22B in our observed PARK7 pathway, we hypothesized that TMED10 might facilitate PARK7 transport into secretory vesicles, potentially including autophagosomes, originating primarily from the ERGIC (53). Surprisingly, the knocking down TMED10 led to increased PARK7 secretion (Fig. 8*A*) without affecting autophagosome formation (as measured by LC3B lipidation, *SI Appendix*, Fig. S6*A*). Additionally, we analyzed the PARK7–LC3B interaction under PARK7-FLAG overexpression conditions by co-IP. HeLa cells transiently transfected with N-terminal FLAG-tagged PARK7 displayed an unchanged secretion ratio of endogenous PARK7 to that of transfected PARK7 upon 6-OHDA treatment (*SI Appendix*, Fig. S6*B*). However, the co-IP experiment did not detect any interaction between PARK7 and LC3B under conditions promoting autophagy with 6-OHDA (*SI Appendix*, Fig. S6*C*). In connection with the TMED10 data, our findings suggest that PARK7 translocation to autophagic transporters might require other mechanisms, particularly for its secretion triggered by 6-OHDA.

Unlike macroautophagy, CMA selectively targets individual cytosolic proteins tagged with a specific amino acid sequence (KFERQ-like motif) by HSPA8 chaperone for their direct delivery to lysosomes via LAMP2A (16). Interestingly, PARK7 possesses

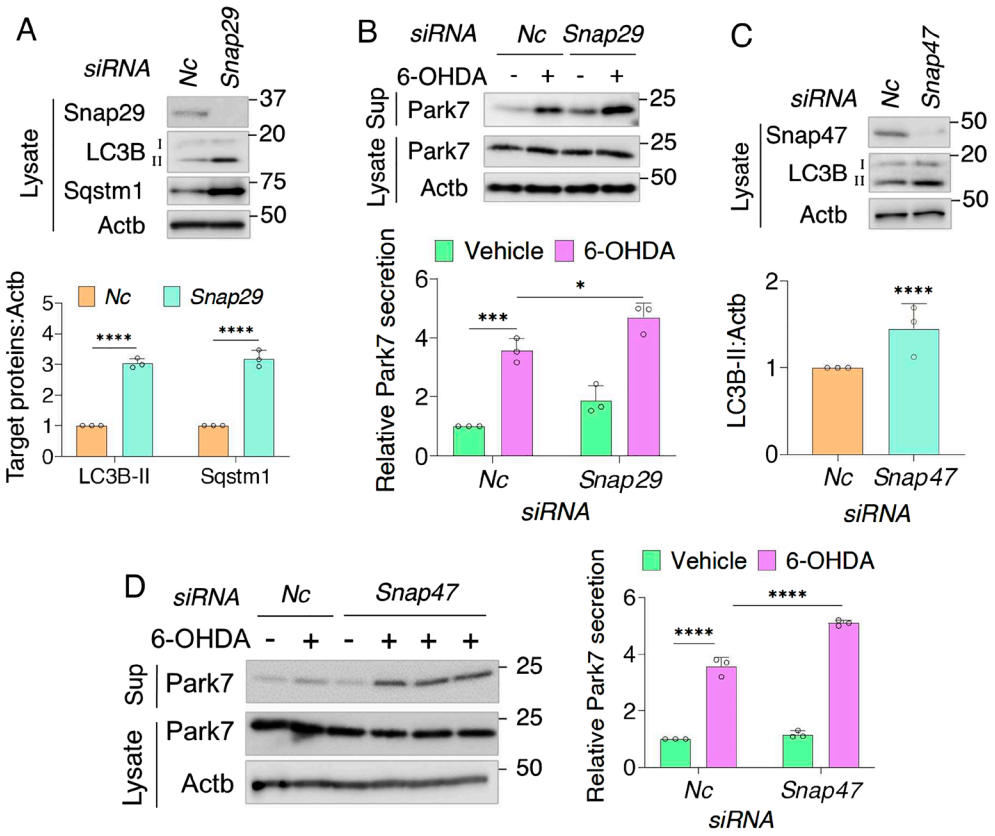

Fig. 5. 6-OHDA-induced PARK7 secretion is independent of STX17-SNAP29 or STX17-SNAP47 SNARE complex mediating autophagosome-lysosome fusion. (*A*) Lysates from MEF cells transfected with siRNAs targeting *Snap29* and *Nc* were analyzed by WB. The bar graph illustrates the relative LC3B-II and Sqstm1 intensities normalized by Actb. *Nc*, negative control. (*B*) MEF cells transfected with siRNAs targeting *Snap29* and *Nc* were treated with 100 μM 6-OHDA and cultured in serum-free DMEM. Lysates and sup were analyzed by WB. The bar graph represents the relative secreted Park7. (*C*) Lysates from MEF cells transfected with siRNAs targeting *Snap47* and *Nc* were analyzed by WB. The bar graph illustrates the relative LC3B-II intensities normalized by Actb. (*D*) MEF cells transfected with siRNAs targeting *Snap47* and *Nc* were treated with 100 μM 6-OHDA and cultured in serum-free DMEM. Lysates and sup were analyzed by WB. The bar graph represents the relative secreted Park7.

four potential CMA motifs (one canonical and three putative) that are evolutionarily conserved across species (*SI Appendix*, Fig. S6*D*). We generated site-directed mutants of PARK7 fused with a FLAG tag, altering critical residues within the canonical motif and two similar motifs (*SI Appendix*, Fig. S6*E*), and measured their secretion levels. WB analysis revealed significantly lowered secretion for three of the four PARK7 mutants (91AA92, 94AA95, and 44AA45), while the endogenous PARK7 and wild-type variant of PARK7-FLAG levels remained unaffected (Fig. 8 *B* and *C*). These findings strongly support the importance of KFERQ-like motifs in PARK7 secretion.

Further investigation into CMA machinery revealed that siRNA knockdown of either HSPA8 or LAMP2 (*SI Appendix*, Fig. S6*F*), essential components of CMA, significantly downregulated PARK7 secretion upon 6-OHDA treatment (Fig. 8*D*). The effectiveness of CMA inhibition was confirmed by the restoration of a known CMA substrate, GPX4, in lysates under the knockdown conditions (*SI Appendix*, Fig. S6*G*). Additionally, IP experiments showed an increased interaction between FLAG-tagged wild-type PARK7 and HSPA8 in response to 6-OHDA stimulation (Fig. 8*E*).

It is essential to consider that PARK7 functions as a homodimer (57), while CMA requires the lysosomal translocation of unfolded, monomeric PARK7. We employed a covalent cross-linker disuccinimidyl suberate (DSS) to preserve the native PARK7 structures and assessed its effect on 6-OHDA treatment. Our data revealed that under 6-OHDA stimulation, intracellular PARK7 remains primarily dimeric, while secreted PARK7 predominantly contained the monomeric form (Fig. 8*F*). Interestingly, under compromised CMA conditions (HSPA8 and LAMP2 knockdown), we observed an accumulation of monomeric PARK7 with a smaller extent of changes in dimer levels in lysates (Fig. 8*G*). These findings suggest PARK7 secretion is favored in the monomeric form, in which a CMA-mediated lysosomal translocation pathway dependent on HSPA8 and LAMP2 is potentially involved.

Discussion

This study presents a unique series of molecular events, selective translocation, and intracellular trafficking processes involved in the autophagy-based unconventional secretion of PARK7 induced by 6-OHDA, as illustrated in Fig. 9. Our investigation into the regulatory mechanisms of PARK7 secretion has yielded three key findings: i) 6-OHDA induces the unconventional secretion of PARK7 in an autophagy-dependent manner, ii) 6-OHDA facilitates the KFERQ-like motif-based selective translocation of cytosolic monomeric PARK7 to the lysosomal lumen, and iii) a dedicated SNARE complex, consisting of SEC22B-STX3/4-VTI1B-STX8, mediates the fusion of secretory autolysosomes containing PARK7 with the plasma membrane.

Our previous study demonstrated that 6-OHDA-derived electrophilic quinone induces oxidative stress by depleting intracellular glutathione levels, activating the AMPK-ULK1 pathway and secretory autophagy (48). While 6-OHDA is primarily recognized as a neurotoxin, it also affects nondopaminergic cells through similar oxidative stress mechanisms (58). Our findings indicate that 6-OHDA induces oxidative stress in HeLa cells, as NAC treatment effectively suppresses 6-OHDA-induced PARK7 secretion. Consistent with our previous report (48), BFA inhibition confirmed that PARK7, as a leaderless cargo, bypasses the ER-Golgi route. Multiple knockdown and knockout experiments targeting key autophagy regulators (ATG5, ATG9, ATG16L1, and FIP200) revealed that autophagic membrane biogenesis is critical for PARK7 secretion. Additionally, rapamycin-mediated autophagy activation significantly enhanced PARK7 secretion. Supporting our findings, previous studies on the unconventional

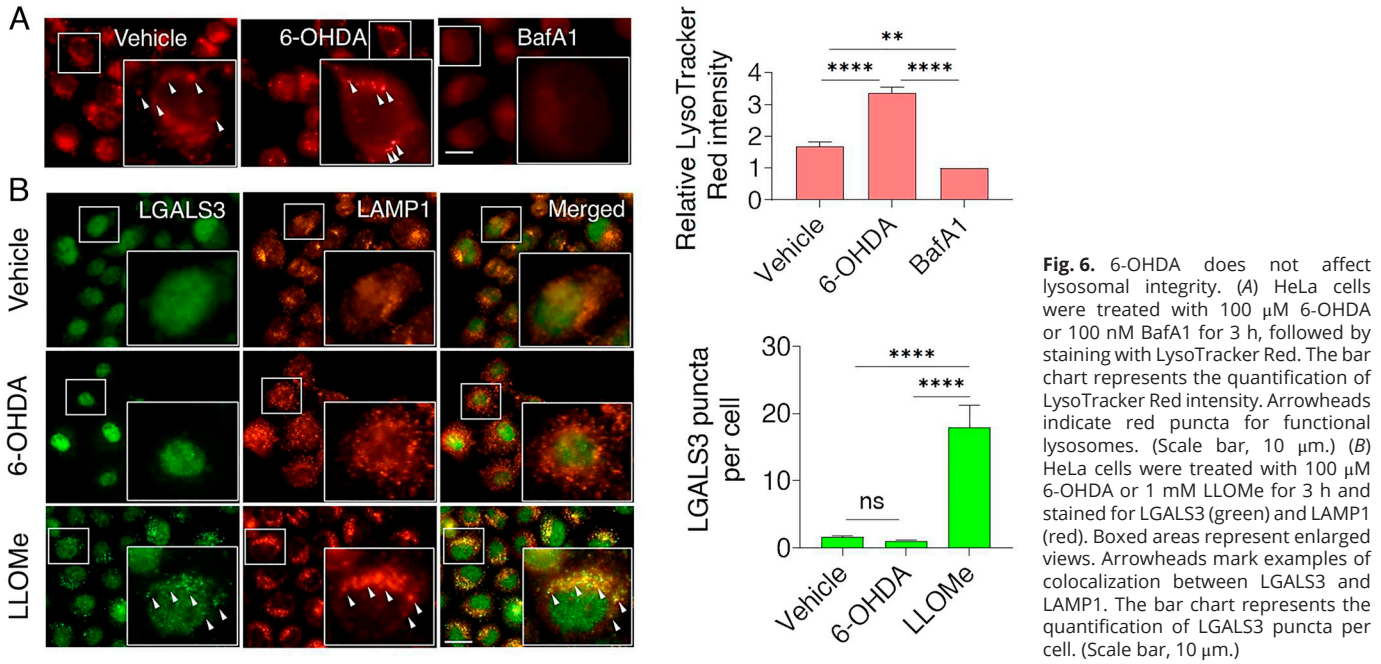

Fig. 6. 6-OHDA does not affect lysosomal integrity. (*A*) HeLa cells were treated with 100 μM 6-OHDA or 100 nM BafA1 for 3 h, followed by staining with LysoTracker Red. The bar chart represents the quantification of LysoTracker Red intensity. Arrowheads indicate red puncta for functional lysosomes. (Scale bar, 10 μm.) (*B*) HeLa cells were treated with 100 μM 6-OHDA or 1 mM LLOMe for 3 h and stained for LGALS3 (green) and LAMP1 (red). Boxed areas represent enlarged views. Arrowheads mark examples of colocalization between LGALS3 and LAMP1. The bar chart represents the quantification of LGALS3 puncta per cell. (Scale bar, 10 μm.)

secretion of insulin-degrading enzyme (IDE) from astrocytes (59) and α-Crystallin B from COS-7 cells (24) rely on mTOR signaling. Since mTOR functions as a key regulator of autophagy in response to nutritional stress, further investigation is warranted to dissect the intricate interplay between mTOR signaling and the regulation of both degradative and secretory autophagy pathways under 6-OHDA-induced oxidative stress and nutrient deprivation conditions.

Unconventionally secreted cargoes utilize diverse mechanisms to access vesicular compartments, including specific transporters, direct incorporation into autophagic structures, or engulfment by MVBs (3). Our fractionation analysis revealed that extracellular PARK7 is not associated with exosomes, unlike mutant huntingtin protein secretion (60). Prior transmission electron microscopy analyses demonstrated that 6-OHDA treatment induces phagophores, autophagosomes, and autolysosomes in MEF cells (48). Our recent findings linked LMP-induced PARK7 secretion to secretory autophagosome (61), prompting us to investigate whether 6-OHDA-induced PARK7 secretion follows a similar route. Inhibition of autophagosome-lysosome fusion or autophagy flux significantly downregulated PARK7 secretion, suggesting that secretory autophagosomes are unlikely to mediate this process. Furthermore, our data do not support TMED10-dependent delivery of PARK7 to secretory vesicles, even those potentially linked to autophagosomes (56). These paradoxical results underscore the context-dependent nature of PARK7 secretion and highlight the necessity to elucidate how distinct cellular stressors, for instance, oxidative damage and lysosomal dysfunction, regulate the autophagy-dependent unconventional secretion of leaderless proteins like PARK7 in a cell-type-specific manner.

Beyond the ubiquitin–proteasome system, which degrades ubiquitin-tagged proteins, CMA selectively targets individual cytosolic proteins for lysosomal degradation. In CMA, cytosolic substrates are directly translocated into the lysosome without vesicle intermediates, involving cytosolic and lysosomal HSPA8 chaperones and lysosomal LAMP2A transporter, which requires protein unfolding (16). Stress conditions like starvation and oxidative stress activate CMA by regulating LAMP2A levels or its oligomerization. Inspired by the selective secretory translocation of IL-1β, we investigated the potential of this route for PARK7, as its protein sequence contains several KFERQ-like motifs conserved across species. Notably, siRNA-based knockdown of chaperones HSPA8, HSP90, and LAMP2 in the IL-1β study suggested a CMA-mediated PARK7 secretion mechanism distinct from CMA for mature IL-1β translocation into vesicles (23). In our experiments, site-directed mutagenesis of KFERQ-like motifs in PARK7 suppressed its secretion, likely due to decreased HSPA8 binding affinity and impaired translocation to the lysosomal lumen. These results highlight an intriguing intersection between the CMA-mediated degradation of PARK7 and its unconventional secretion under stress conditions.

Previous research suggests that CMA targets extensively oxidized PARK7 for lysosomal degradation, a process critical for maintaining mitochondrial homeostasis (62). Our findings indicate that 6-OHDA-induced oxidative stress triggers the selective secretion of monomeric PARK7, while CMA impairment via HSPA8 and LAMP2 knockdown leads to its intracellular accumulation. This dual role of lysosomes in PARK7 regulation suggests a dynamic balance between protein quality control and unconventional secretion. Oxidative stress likely disrupts the PARK7 homodimer, exposing KFERQ-like motifs that facilitate HSPA8 binding (62) and LAMP2-dependent trafficking. However, alternative mechanisms for stress-induced PARK7 monomerization cannot be excluded. For example, exposure to 6-OHDA may cleave PARK7 homodimers by revealing protease-sensitive regions or exposing hydrophobic surfaces, which could attract small heat shock proteins for temporary stabilization before HSPA8 recognition (63).

Further investigation is necessary to determine why increased autophagic flux is critical for PARK7 secretion when CMA facilitates translocation into the lysosomal lumen. One possibility is that 6-OHDA-induced autophagic flux supports the formation of autophagosomes and autolysosomes, ensuring the availability of the autophagic machinery required for PARK7 secretion. Additionally, this flux may promote crosstalk between autophagy and CMA through 6-OHDA-regulated stress signaling pathways. To elucidate the role of autophagic flux in PARK7 secretion, future studies could assess PARK7 lysosomal translocation in autophagy-deficient models such as STX17$^{-/-}$ or FIP200$^{-/-}$ cells using lysosomal fractionation or Lyso-IP analysis. Since these models do not directly impair lysosomal function, PARK7

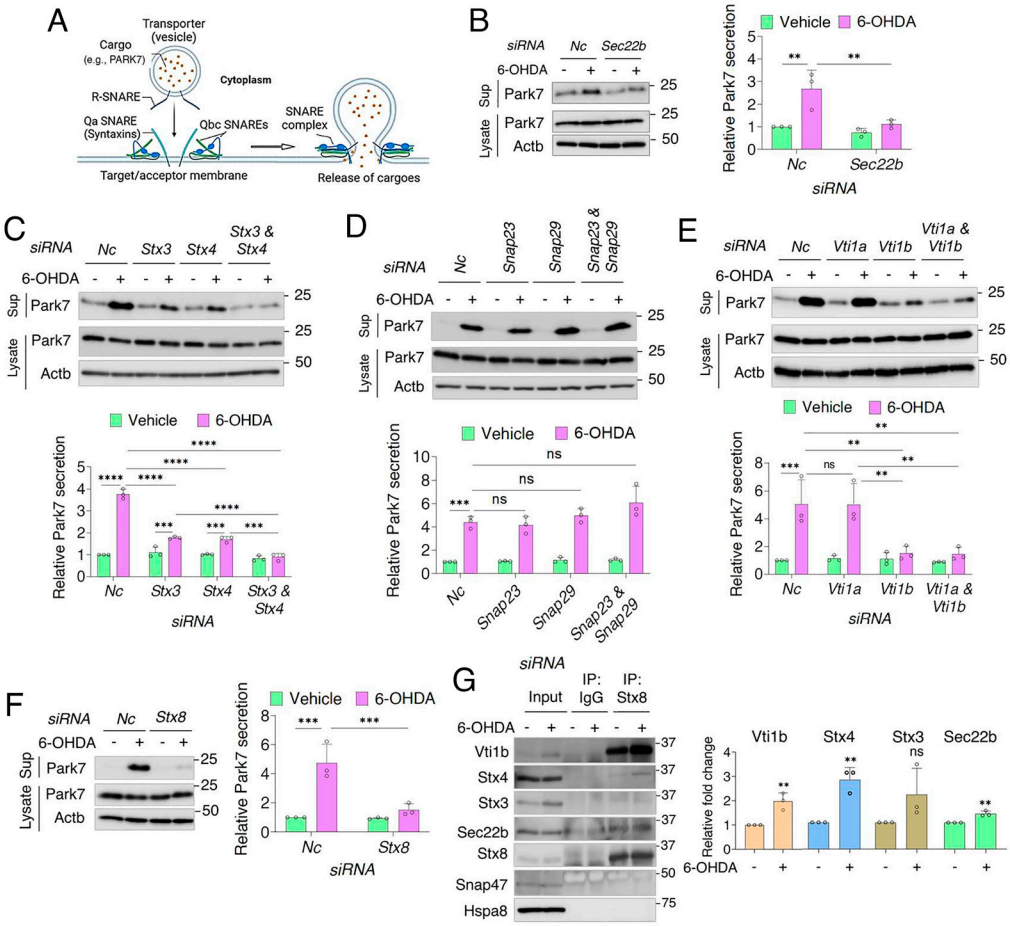

Fig. 7. A unique set of SNARE members mediates PARK7 release in the extracellular environment. (*A*) Schematic representation of the QabcR–SNARE complex driving membrane fusion and cargo trafficking. (*B–F*) MEF cells transfected with siRNAs targeting (*B*) *Sec22b*, (*C*) *Stx3* or *Stx4* or in combination, (*D*) *Snap23* or *Snap29* or in combination, (*E*) *Vti1a* or *Vti1b* or in combination, and (*F*) *Stx8* were treated with 100 μM 6-OHDA and cultured in serum-free DMEM. Lysates and sup were analyzed by WB for the indicated proteins. The bar graphs represent the relative secreted Park7. *Nc*, negative control. (*G*) MEF cells were treated with 100 μM 6-OHDA. Lysates were immunoprecipitated with an anti-Stx8 antibody and analyzed by WB. The bar chart represents the relative fold change of the coprecipitated proteins.

lysosomal translocation should, in principle, remain unaffected. However, if PARK7 undergoes CMA-mediated degradation rather than secretion in these systems, it would further support that autophagic flux is indispensable for its unconventional secretion. A crucial unresolved question is whether autophagic flux is required for both lysosomal PARK7 translocation and secretion or is it involved explicitly in SNARE-mediated fusion of PARK7-containing secretory autolysosomes with the plasma membrane. Resolving this issue could provide fundamental mechanistic insights into PARK7 secretion. Identifying distinct secretory autolysosomal markers and analyzing PARK7 colocalization within these compartments through immunogold electron microscopy could offer definitive evidence to strengthen our findings.

Moreover, the mechanisms enabling lysosomal PARK7 to evade degradation remain unclear. Our observation that approximately 10% of total PARK7 is secreted upon 6-OHDA stimulation (48) suggests that while lysosomes primarily function to degrade translocated PARK7 for cellular homeostasis, they may selectively secrete excess PARK7 beyond a regulatory threshold. Factors governing this balance between degradation and secretion remain unknown. Another intriguing aspect is the observed fusion between PARK7-containing lysosomes and autophagosomes. Whether this interaction enhances secretion efficiency or is merely a byproduct of lysosome-autophagosome crosstalk warrants further investigation. Elucidating these regulatory mechanisms could provide valuable insights into the unconventional secretion of PARK7 and its broader physiological relevance.

Secretory autophagy, often triggered by cellular stress, mediates the release of cargoes such as IL-1β via membrane-bound vesicles that fuse directly with the plasma membrane, bypassing lysosomal degradation (18). Notably, the secretion of these cargoes remains unaffected by STX17 knockdown, supporting a lysosome-independent mechanism. Further evidence includes the lack of colocalization between α-Crystallin B in LC3-positive compartments and the lysosomal marker LAMP1 (24) and enhanced HMGB1 secretion under conditions that inhibit autolysosome formation (25). These findings collectively highlight an unconventional secretory pathway distinct from lysosomal involvement. In contrast, the secretion of several cargoes, including IDE (59), transforming growth factor beta 1 (64), and mutant huntingtin (65), requires lysosomal integrity. Lysosomal disruption via BafA1 downregulates the release of these proteins, which contain KFERQ-like motifs in their sequences, suggesting a pathway potentially overlapping with 6-OHDA-induced PARK7 secretion. Our observations confirm that 6-OHDA treatment does not compromise lysosomal integrity like LMP-induced secretion. Furthermore, inhibiting lysosomal interactions with autophagosomes through STX17 knockdown/knockout, interfering with lysosomal degradative functions by BafA1 or CQ, hindering lysosomal translocation of PARK7 by

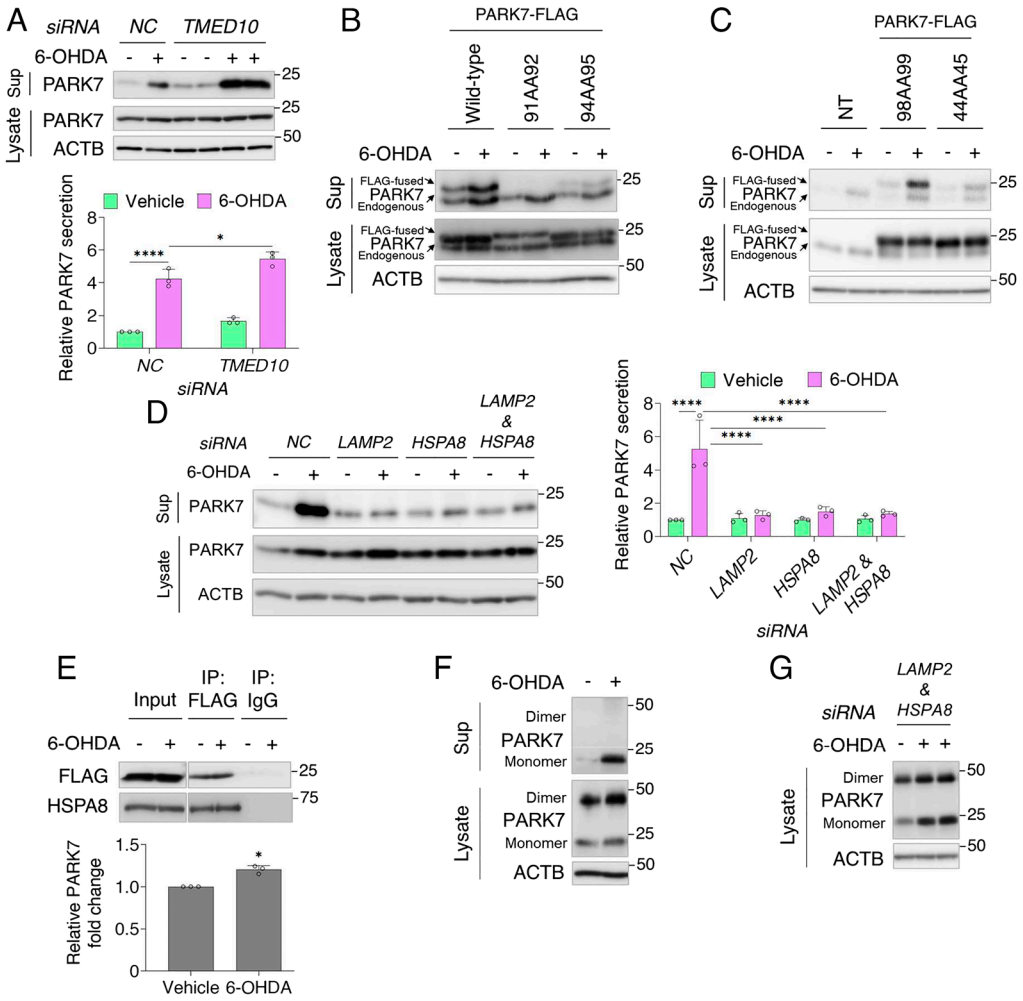

Fig. 8. KFERQ-like motifs contribute to PARK7 secretion via CMA. (*A*) HeLa cells transfected with siRNAs targeting *TMED10* or *NC* were treated with 100 μM 6-OHDA and cultured in serum-free DMEM. Lysates and sup were analyzed by WB. The bar graph represents the relative secreted PARK7. *NC*, negative control. (*B* and *C*) HeLa cells transiently transfected with PARK7-FLAG or mutant PARK7 (91AA92, 94AA95, 98AA99, and 44AA45)-FLAG plasmids were treated with 100 μM 6-OHDA and cultured in serum-free DMEM. Lysates and sup were analyzed by WB. The bar graphs represent the relative secreted PARK7. NT, nontransfected. (*D*) HeLa cells transfected with siRNAs targeting *LAMP2* or *HSPA8* or in combination were treated with 100 μM 6-OHDA and cultured in serum-free DMEM. Lysates and sup were analyzed by WB. The bar graph represents the relative secreted PARK7. (*E*) HeLa cells transiently transfected with PARK7-FLAG were treated with 100 μM 6-OHDA. Lysates were immunoprecipitated with the anti-FLAG antibody and samples were analyzed by WB. The bar chart represents the relative fold change of PARK7. (*F*) HeLa cells were treated with 100 μM 6-OHDA and cultured in serum-free DMEM. Lysates and sup were cross-linked with DSS, and samples were analyzed by WB. (*G*) HeLa cells transfected with siRNAs targeting *LAMP2* and *HSPA8* were treated with 100 μM 6-OHDA. Lysates were cross-linked with DSS, and samples were analyzed by WB.

mutating its KFERQ motifs, or knocking down CMA components all consistently suppressed 6-OHDA-induced PARK7 secretion. These results firmly indicate that lysosomal functionality and structural integrity are indispensable for PARK7 secretion under these conditions.

Upon stress, cells can activate lysosomal exocytosis (66), a process in which secretory lysosomes fuse with the plasma membrane to release their contents extracellularly. This process involves a SNARE complex comprising the plasma membrane SNAREs SNAP23 and STX4 and the lysosomal SNARE VAMP7 (67). However, our knockdown experiments targeting SNAP23 revealed no impact on 6-OHDA-induced PARK7 secretion, excluding lysosomal exocytosis as a pathway for PARK7 release. Our findings highlight the critical roles of autophagosome biogenesis, lysosomal activity, and autophagosome-lysosome fusion in mediating PARK7 secretion under 6-OHDA stress. Based on these observations, we propose the concept of "secretory autolysosome-mediated secretion" as the mechanism driving 6-OHDA-induced PARK7 release. Future studies should explore whether 6-OHDA regulates molecular switches that divert PARK7-containing lysosomes toward secretion rather than degradation.

Secretory and degradative autophagy share core ATG proteins but differ in destination: degradative autophagosomes fuse with lysosomes, while secretory autophagosomes fuse with the plasma membrane (68). Despite similarities in cargo machinery biogenesis, they employ distinct transport mechanisms, tethers, and SNARE proteins. The SNARE complex, composed of Qa, Qb, Qc, and R-SNAREs, is crucial for intracellular membrane fusion, playing a vital role in the final stages of docking and fusion across various vesicle-mediated transport events (19). Our findings emphasize the roles of both SEC22B and STX17 in PARK7 secretion, suggesting their interplay in secretory autophagic pathways. Additionally, our results suggest specific SNAREs mediating autophagosome-lysosome fusion in 6-OHDA-induced PARK7 secretion. Interestingly, interfering with neither of the conventional SNARE pairs—STX17-SNAP29, which mediates starvation-induced bulk autophagy (14), nor STX17-SNAP47, which operates in selective autophagy under nonstarvation conditions (69)—-downregulated PARK7 secretion

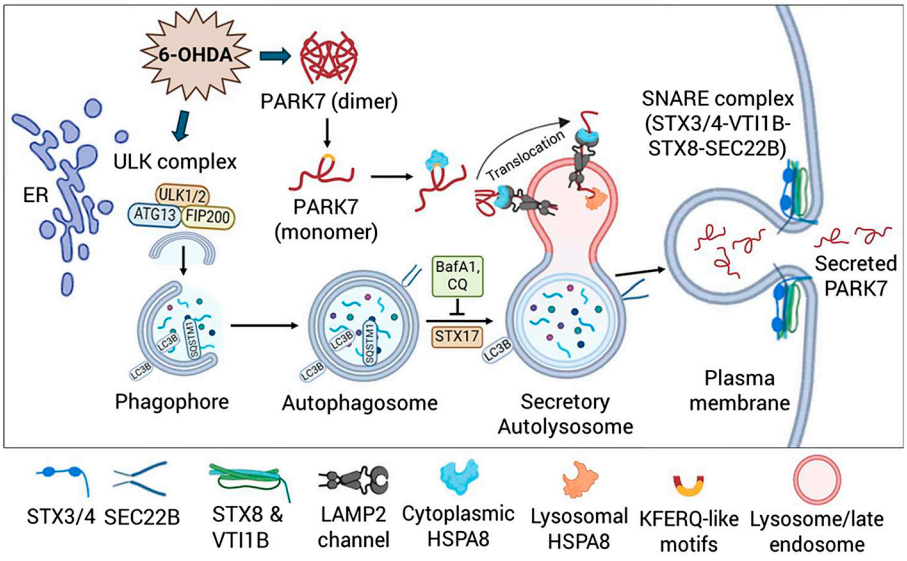

Fig. 9. Proposed model of 6-OHDA-induced autophagy-based unconventional PARK7 secretion. Oxidative stress induced by 6-OHDA stimulates autophagy flux, which enhances STX17-mediated autolysosome formation, leading to the degradation of autophagosomal contents. However, in response to autophagy promotion by 6-OHDA, a subset of autophagosomes recruits ERGIC R-SNARE SEC22B. The KFERQ-like motifs of monomeric PARK7 selectively bind to HSPA8 chaperones and are recruited to the lysosomal membrane, followed by translocation into the lysosomal lumen via the LAMP2 channel. A pool of PARK7-containing lysosomes fuses with SEC22B-containing autophagosomes to form secretory autolysosomes, which then fuse with the plasma membrane mediated by a unique QabcR–SNARE complex comprising STX3/4, VTI1B, STX8, and SEC22B, releasing PARK7 into the extracellular matrix.

in our system. These observations suggest that STX17 may require a dedicated SNARE partner to facilitate the selective fusion of autophagosomes with lysosomes, forming secretory autolysosomes. Furthermore, the possibility that STX17 contributes to PARK7 secretion through an alternative mechanism, independent of its role in autolysosome formation, cannot be ruled out. Further investigation is required to elucidate its precise function in the unconventional secretion of PARK7.

Furthermore, our study identified a SNARE complex composed of SEC22B, STX3/4, VTI1B, and STX8 that mediates the fusion of PARK7-containing secretory autolysosomes with the plasma membrane, facilitating PARK7 secretion. Unlike the SEC22B-SNAP23/29-STX3/4 complex in immune cells (21), this SNARE combination represents a distinct secretory autophagy mechanism. Co-IP assays confirmed interactions among these SNARE members, supported by AlphaFold multimer predictions. Nevertheless, direct biochemical validation of these interactions remains an open question and requires further investigation.

In the current study, we identified a CMA-mediated selective lysosomal translocation pathway that regulates the oxidative stress-induced secretion of the leaderless cytosolic protein PARK7. Notably, this autophagy-based unconventional secretion appears specific to cargoes containing KFERQ-like motifs, as HSPA8 recognizes these motifs for cargo selection and translocation to lysosomes. Further studies are necessary to determine whether this pathway applies to other KFERQ-like motif-containing proteins under cellular stress. Investigating the physiological and pathological implications of this mechanism could provide valuable insights into PARK7-related disorders and facilitate the development of targeted therapeutic strategies aimed at modulating PARK7 secretion.

Materials and Methods

Cell Culture. HeLa (wild-type, STX17$^{-/-}$, and FIP200$^{-/-}$) (70) and MEF (71) cells were used in this study. All cell lines were cultured in high-glucose Dulbecco's modified Eagle's medium (DMEM, 044-29765, FUJIFILM Wako) supplemented with 10% heat-inactivated fetal bovine serum (FBS, 175012, Nichirei Bioscience) and 1% penicillin-streptomycin (168-23191, FUJIFILM Wako) in a humidified incubator with 5% CO_2 at 37 °C. Gene and protein nomenclature were standardized according to species-specific guidelines: human names follow the HUGO Gene Nomenclature Committee, and mouse names adhere to the International Committee on Standardized Genetic Nomenclature for Mice. Human gene/protein designations were prioritized in cases of common terminology to ensure consistency.

The rest of the methods are available in *SI Appendix*.

Data, Materials, and Software Availability. All study data are included in the article and/or *SI Appendix*.

ACKNOWLEDGMENTS. We thank Dr. Tamotsu Yoshimori and Dr. Tatsuya Kaminishi (Osaka University, Japan), and Dr. Shigeo Takamori (Doshisha University, Japan) for their valuable suggestions on the study. We thank Dr. Tamotsu Yoshimori (Osaka University, Japan) and Dr. Noboru Mizushima (The University of Tokyo, Japan) for cell lines. We thank Dr. Kohei Matsuda (Systems Life Sciences Laboratory, Doshisha University) for preparing the pcDNA3.1-αFLAG-tagged-human PARK7 plasmids used in this study. Schematic diagrams in Figs. 7*A* and 9 were created using BioRender (www.biorender.com).

Author affiliations: [a]Systems Life Sciences Laboratory, Graduate School of Life and Medical Sciences, Doshisha University, Kyotanabe 610-0394, Kyoto, Japan; and [b]Systems Life Sciences Laboratory, Department of Medical Life Systems, Faculty of Life and Medical Sciences, Doshisha University, Kyotanabe 610-0394, Kyoto, Japan

Author contributions: B.K.D., Y.U., and N.N. designed research; B.K.D. performed research; Y.M., Y.A., and R.H. contributed new reagents/analytic tools; B.K.D., Y.U., and N.N. analyzed data; B.K.D. wrote the original draft; B.K.D., Y.U., and N.N. reviewed and edited the final paper; and B.K.D. and Y.U. wrote the paper.

1. W. Nickel, Pathways of unconventional protein secretion. *Curr. Opin. Biotechnol.* **21**, 621–626 (2010).
2. C. Rabouille, V. Malhotra, W. Nickel, Diversity in unconventional protein secretion. *J. Cell Sci.* **125**, 5251–5255 (2012).
3. M. J. Cohen, W. J. Chirico, P. N. Lipke, Through the back door: Unconventional protein secretion. *Cell Surf.* **6**, 100045 (2020).
4. N. Mizushima, B. Levine, A. M. Cuervo, D. J. Klionsky, Autophagy fights disease through cellular self-digestion. *Nature* **451**, 1069–1075 (2008).
5. T. Nishimura, S. A. Tooze, Emerging roles of ATG proteins and membrane lipids in autophagosome formation. *Cell Discov.* **6**, 32 (2020).
6. J. Kim, M. Kundu, B. Viollet, K.-L. Guan, AMPK and mTOR regulate autophagy through direct phosphorylation of Ulk1. *Nat. Cell Biol.* **13**, 132–141 (2011).
7. R. C. Russell *et al.*, ULK1 induces autophagy by phosphorylating Beclin-1 and activating VPS34 lipid kinase. *Nat. Cell Biol.* **15**, 741–750 (2013).
8. D. F. Egan *et al.*, Phosphorylation of ULK1 (hATG1) by AMP-activated protein kinase connects energy sensing to mitophagy. *Science* **331**, 456–461 (2011).
9. E. L. Axe *et al.*, Autophagosome formation from membrane compartments enriched in phosphatidylinositol 3-phosphate and dynamically connected to the endoplasmic reticulum. *J. Cell Biol.* **182**, 685–701 (2008).
10. N. Fujita *et al.*, The Atg16L complex specifies the site of LC3 lipidation for membrane biogenesis in autophagy. *Mol. Biol. Cell* **19**, 2092–2100 (2008).
11. Y. Kabeya *et al.*, LC3, a mammalian homologue of yeast Apg8p, is localized in autophagosome membranes after processing. *EMBO J.* **19**, 5720–5728 (2000).
12. N. Fujita *et al.*, Recruitment of the autophagic machinery to endosomes during infection is mediated by ubiquitin. *J. Cell Biol.* **203**, 115–128 (2013).
13. R. Liu, X. Zhi, Q. Zhong, ATG14 controls SNARE-mediated autophagosome fusion with a lysosome. *Autophagy* **11**, 847–849 (2015).

14. E. Itakura, C. Kishi-Itakura, N. Mizushima, The hairpin-type tail-anchored SNARE syntaxin 17 targets to autophagosomes for fusion with endosomes/lysosomes. *Cell* **151**, 1256–1269 (2012).
15. T. Johansen, T. Lamark, Selective autophagy mediated by autophagic adapter proteins. *Autophagy* **7**, 279–296 (2011).
16. F. A. Agarraberes, J. F. Dice, A molecular chaperone complex at the lysosomal membrane is required for protein translocation. *J. Cell Sci.* **114**, 2491–2499 (2001).
17. U. Bandyopadhyay, S. Kaushik, L. Varticovski, A. M. Cuervo, The chaperone-mediated autophagy receptor organizes in dynamic protein complexes at the lysosomal membrane. *Mol. Cell. Biol.* **28**, 5747–5763 (2008).
18. N. Dupont *et al.*, Autophagy-based unconventional secretory pathway for extracellular delivery of IL-1β. *EMBO J.* **30**, 4701–4711 (2011).
19. M. Ponpuak *et al.*, Secretory autophagy. *Curr. Opin. Cell Biol.* **35**, 106–116 (2015).
20. X. Hou, J. O. Watzlawik, F. C. Fiesel, W. Springer, Autophagy in Parkinson's disease. *J. Mol. Biol.* **432**, 2651–2672 (2020).
21. T. Kimura *et al.*, Dedicated SNAREs and specialized TRIM cargo receptors mediate secretory autophagy. *EMBO J.* **36**, 42–60 (2017).
22. J. M. Duran, C. Anjard, C. Stefan, W. F. Loomis, V. Malhotra, Unconventional secretion of Acb1 is mediated by autophagosomes. *J. Cell Biol.* **188**, 527–536 (2010).
23. M. Zhang, S. J. Kenny, L. Ge, K. Xu, R. Schekman, Translocation of interleukin-1β into a vesicle intermediate in autophagy-mediated secretion. *eLife* **4**, e11205 (2015).
24. M. D'Agostino *et al.*, Unconventional secretion of α-Crystallin B requires the autophagic pathway and is controlled by phosphorylation of its serine 59 residue. *Sci. Rep.* **9**, 16892 (2019).
25. Y. H. Kim *et al.*, Secretory autophagy machinery and vesicular trafficking are involved in HMGB1 secretion. *Autophagy* **17**, 2345–2362 (2021).
26. A. R. Wagh, P. Sulakshane, M. H. Glickman, Alzheimer's disease-associated mutant ubiquitin (UBB+1) is secreted through an autophagosome-like vesicle-mediated unconventional pathway *Biochim. Biophys. Acta: Gene Regul. Mech.* **1866**, 194936 (2023).
27. H. Ariga, S. M. M. Iguchi-Ariga, *DJ-1/PARK7 Protein, The multifaceted roles of DJ-1 as an antioxidant*. H. Ariga, S. M. M. Iguchi-Ariga, Eds. (Springer, Singapore, 2017).
28. T. Taira *et al.*, DJ-1 has a role in antioxidative stress to prevent cell death. *EMBO Rep.* **5**, 213–218 (2004).
29. T. Yokota *et al.*, Down regulation of DJ-1 enhances cell death by oxidative stress, ER stress, and proteasome inhibition. *Biochem. Biophys. Res. Commun.* **312**, 1342–1348 (2003).
30. B. K. Dash, Y. Urano, Y. Saito, N. Noguchi, Redox-sensitive DJ-1 protein: An insight into physiological roles, secretion, and therapeutic target. *Redox Exp. Med.* **2022**, R96–R115 (2022).
31. N. Lev, D. Ickowicz, E. Melamed, D. Offen, Oxidative insults induce DJ-1 upregulation and redistribution: Implications for neuroprotection. *Neurotoxicology* **29**, 397–405 (2008).
32. N. Zhong *et al.*, DJ-1 transcriptionally up-regulates the human tyrosine hydroxylase by inhibiting the sumoylation of pyrimidine tract-binding protein-associated splicing factor. *J. Biol. Chem.* **281**, 20940–20948 (2006).
33. J. A. Olzmann *et al.*, Familial Parkinson's disease-associated L166P mutation disrupts DJ-1 protein folding and function. *J. Biol. Chem.* **279**, 8506–8515 (2004).
34. H. Gao *et al.*, DJ-1 protects dopaminergic neurons against rotenone-induced apoptosis by enhancing ERK-dependent mitophagy. *J. Mol. Biol.* **423**, 232–248 (2012).
35. J. Blackinton *et al.*, Post-transcriptional regulation of mRNA associated with DJ-1 in sporadic Parkinson disease. *Neurosci. Lett.* **452**, 8–11 (2009).
36. I. Kato *et al.*, Oxidized DJ-1 inhibits p53 by sequestering p53 from promoters in a DNA-binding affinity-dependent manner. *Mol. Cell. Biol.* **33**, 340–359 (2013).
37. T. Yanagida *et al.*, Oxidative stress induction of DJ-1 protein in reactive astrocytes scavenges free radicals and reduces cell injury. *Oxid. Med. Cell. Longev.* **2**, 36–42 (2009).
38. Y. Kaneko *et al.*, DJ-1 ameliorates ischemic cell death in vitro possibly via mitochondrial pathway. *Neurobiol. Dis.* **62**, 56–61 (2014).
39. J.-M. Kim *et al.*, DJ-1 promotes angiogenesis and osteogenesis by activating FGF receptor-1 signaling. *Nat. Commun.* **3**, 1296 (2012).
40. S. Koide-Yoshida *et al.*, DJ-1 degrades transthyretin and an inactive form of DJ-1 is secreted in familial amyloidotic polyneuropathy. *Int. J. Mol. Med.* **19**, 885–893 (2007).
41. F. Le Naour *et al.*, Proteomics-based identification of RS/DJ-1 as a novel circulating tumor antigen in breast cancer. *Clin. Cancer Res.* **7**, 3328–3335 (2001).
42. B. Tsuchiya *et al.*, Clinical significance of DJ-1 as a secretory molecule: Retrospective study of DJ-1 expression at mRNA and protein levels in ductal carcinoma of the breast. *Histopathology* **61**, 69–77 (2012).
43. M. Oda *et al.*, High levels of DJ-1 protein in nipple fluid of patients with breast cancer. *Cancer Sci.* **103**, 1172–1176 (2012).
44. L. Allard *et al.*, PARK7 and nucleoside diphosphate kinase A as plasma markers for the early diagnosis of stroke. *Clin. Chem.* **51**, 2043–2051 (2005).
45. M. Pardo *et al.*, The characterization of the invasion phenotype of uveal melanoma tumour cells shows the presence of MUC18 and HMG-1 metastasis markers and leads to the identification of DJ-1 as a potential serum biomarker. *Int. J. Cancer* **119**, 1014–1022 (2006).
46. M. Waragai *et al.*, Plasma levels of DJ-1 as a possible marker for progression of sporadic Parkinson's disease. *Neurosci. Lett.* **425**, 18–22 (2007).
47. M. Hirotani *et al.*, Correlation between DJ-1 levels in the cerebrospinal fluid and the progression of disabilities in multiple sclerosis patients. *Mult. Scler. J.* **14**, 1056–1060 (2008).
48. Y. Urano *et al.*, 6-Hydroxydopamine induces secretion of PARK7/DJ-1 via autophagy-based unconventional secretory pathway. *Autophagy* **14**, 1943–1958 (2018).
49. M. Mauthe *et al.*, Chloroquine inhibits autophagic flux by decreasing autophagosome–lysosome fusion. *Autophagy* **14**, 1435–1455 (2018).
50. C. Mauvezin, P. Nagy, G. Juhász, T. P. Neufeld, Autophagosome–lysosome fusion is independent of V-ATPase-mediated acidification. *Nat. Commun.* **61**, 1–14 (2015).
51. S. Kimura, T. Noda, T. Yoshimori, Dissection of the autophagosome maturation process by a novel reporter protein, tandem fluorescent-tagged LC3. *Autophagy* **3**, 452–460 (2007).
52. T. Hara *et al.*, FIP200, a ULK-interacting protein, is required for autophagosome formation in mammalian cells. *J. Cell Biol.* **181**, 497–510 (2008).
53. L. Ge, D. Melville, M. Zhang, R. Schekman, The ER–Golgi intermediate compartment is a key membrane source for the LC3 lipidation step of autophagosome biogenesis. *eLife* **2**, e00947 (2013).
54. T. Becker, A. Volchuk, J. E. Rothman, Differential use of endoplasmic reticulum membrane for phagocytosis in J774 macrophages. *Proc. Natl. Acad. Sci. U.S.A.* **102**, 4022–4026 (2005).
55. R. Evans *et al.*, Protein complex prediction with AlphaFold-Multimer. bioRxiv [Preprint] (2022). https://doi.org/10.1101/2021.10.04.463034 (Accessed 15 April 2024).
56. M. Zhang *et al.*, A translocation pathway for vesicle-mediated unconventional protein secretion. *Cell* **181**, 637–652.e15 (2020).
57. V. Bonifati *et al.*, Mutations in the DJ-1 gene associated with autosomal recessive early-onset Parkinsonism. *Science* **299**, 256–259 (2003).
58. P. P. Michel, F. Hefti, Toxicity of 6-hydroxydopamine and dopamine for dopaminergic neurons in culture. *J. Neurosci. Res.* **26**, 428–435 (1990).
59. S. M. Son *et al.*, Insulin-degrading enzyme secretion from astrocytes is mediated by an autophagy-based unconventional secretory pathway in Alzheimer disease. *Autophagy* **12**, 784–800 (2016).
60. R. Bonavita *et al.*, The HSPB1-p62/SQSTM1 functional complex regulates the unconventional secretion and transcellular spreading of the HD-associated mutant huntingtin protein. *Hum. Mol. Genet.* **32**, 2269–2291 (2023).
61. B. K. Dash, Y. Urano, N. Noguchi, Lysosomal damage promotes autophagy-based unconventional secretion of the Parkinson's disease protein PARK7. *Redox Exp. Med.* **2024**, e240014 (2024).
62. B. Wang *et al.*, Essential control of mitochondrial morphology and function by chaperone-mediated autophagy through degradation of PARK7. *Autophagy* **12**, 1215–1228 (2016).
63. S. Sharma, P. Christen, P. Goloubinoff, Disaggregating chaperones: An unfolding story. *Curr. Protein Pept. Sci.* **10**, 432–446 (2009).
64. J. Nüchel *et al.*, TGFB1 is secreted through an unconventional pathway dependent on the autophagic machinery and cytoskeletal regulators. *Autophagy* **14**, 465–486 (2018).
65. E. Ahat *et al.*, GRASP55 regulates the unconventional secretion and aggregation of mutant huntingtin. *J. Biol. Chem.* **298**, 102219 (2022).
66. C. Andrei *et al.*, The secretory route of the leaderless protein interleukin 1β involves exocytosis of endolysosome-related vesicles. *Mol. Biol. Cell* **10**, 1463–1475 (1999).
67. S. K. Rao, C. Huynh, V. Proux-Gillardeaux, T. Galli, N. W. Andrews, Identification of SNAREs involved in synaptotagmin VII-regulated lysosomal exocytosis. *J. Biol. Chem.* **279**, 20471–20479 (2004).
68. S. Padmanabhan, R. Manjithaya, Facets of autophagy based unconventional protein secretion–The road less traveled. *Front. Mol. Biosci.* **7**, 273 (2020).
69. F. Jian *et al.*, The STX17–SNAP47–VAMP7/VAMP8 complex is the default SNARE complex mediating autophagosome–lysosome fusion. *Cell Res.* **34**, 151–168 (2024).
70. S. Nakamura *et al.*, LC3 lipidation is essential for TFEB activation during the lysosomal damage response to kidney injury. *Nat. Cell Biol.* **2210**, 1252–1263 (2020).
71. A. Kuma *et al.*, The role of autophagy during the early neonatal starvation period. *Nature* **432**, 1032–1036 (2004).